Diffractive Optics: Design, Realization, and Applications

E. HASMAN
N. DAVIDSON
Y. DANZIGER
A. A. FRIESEM

Department of Physics of Complex Systems
Weizmann Institute of Science
Rehovot, Israel

This paper presents methods for designing and recording optimal computer-generated diffractive optical elements. The design method is based on an analytic ray-tracing procedure for minimizing aberrations. The recording involves computer-generated masks and multiple lithographic processes in order to form reflective and transmissive multilevel, surface relief-phase, diffractive elements. As a result, the elements can have high diffraction efficiencies over a broad range of incidence angles. Even generalized diffractive elements that operate with highly uniform diffraction efficiency and polychromatic radiation can be designed and recorded by optimizing the shape and height of the relief gratings. To illustrate the effectiveness of the diffractive optical elements, they have been incorporated into a number of applications, involving visible as well as infra-red radiation. Some that deal with coordinate transformation, beam shaping, and polarization control are briefly reviewed.

Keywords computer-generated holograms, diffractive optical elements, holographic optical elements, kinoform, multilevel diffractive elements, relief gratings, wavefront shaping

One of the most successful and viable outgrowths of holography [1–5] involves *holographic optical elements* (HOEs) [6], known, more generally, as *diffractive optical elements* (DOEs). The DOEs diffract light from a generalized grating structure having nonuniform groove spacing. They can be formed as a thin optical element that can provide unique functions and configurations. As such, they can replace very complex conventional spheric and aspheric optical elements, like glass lenses and mirrors, which work on the principles of refraction and reflection. Moreover, DOEs can offer optical properties that are not possible with conventional optics.

Computers have played the most important role in the development of DOEs. Specifically, *computer-generated holograms* (CGHs) can behave as very sophisticated optical elements. The CGHs, namely synthetic holograms, represent a class of holograms that are produced as graphical output from a digital computer [7–10]. Given a mathematical description of a wavefront or an object represented by an

Address correspondence to E. Hasman, Department of Physics of Complex Systems, Weizmann Institute of Science, Rehovot 76100, Israel. E-mail: fehasman@weizmann.weizmann.ac.il

Fiber and Integrated Optics, 16:1–25, 1997

0146-8030/97 $12.00 + .00

array of points, the computer can calculate the amplitude transmittance of the hologram and plot it by means of a laser printer or an electron-beam recorder.

To optimize the performance of DOEs, it is necessary to deal with two independent problems separately. One involves the design of the grating functions so as to minimize the aberrations, and the other involves the appropriate recording method so as to obtain high diffraction efficiencies. In this paper, we present a design optimization method that is suitable for a general class of DOEs. This method is based on an analytic ray-tracing procedure that minimizes the mean-squared difference of the propagation vector components between the actual output wavefronts and the desired output wavefronts. The minimization yields integral equations for the grating vector components that can be solved analytically, in some cases without any approximation. This results in a well-behaved grating function that defines a DOE. We also present techniques for obtaining high diffraction efficiencies. These include multilevel phase holograms, whose efficiencies approach the ideal kinoform, blazed grating, efficiency [11], and heterostructure optical elements, with accurate discrete multilevel. We then extend the design and recording methods to include computer-generated multilevel diffractive elements, in which the phase and the amplitude of the output wavefront can be controlled independently.

Finally, we describe how DOEs can be exploited for optical transformation and wavefront shaping. Specific examples include annular-to-circular beam transformation, nondiffracting beams, hybrid diffractive-refractive achromats, multiple beam grating, a novel aspheric Axilens for achieving extended focal depth while keeping high lateral resolution, and space-variant polarization elements.

Analytic Ray-Tracing Design Procedure

In general, DOEs can have a relatively large amount of aberrations [6]. Fortunately, these aberrations can be minimized by restoring to optimization procedures when designing the grating functions of the DOEs [12–14]. In the following, we shall present a relatively general design optimization procedure.

Typically, a DOE can be described as a diffractive grating that transforms the phase of an incoming wavefront to another output phase. The phase of the output wavefront, $\phi_o(x, y)$, for the first diffracted order is given by

$$\phi_o(x, y) = \phi_i(x, y) - \phi_h(x, y) \tag{1}$$

where $\phi_i(x, y)$ is the phase of the input wavefront and $\phi_h(x, y)$ is the grating function of the DOE.

In our design procedure, we exploit the normalized propagation vectors and grating vector of the DOE rather than the phases. The normalized propagation vectors, which can be regarded as the direction cosines of the input ($\hat{\bar{K}}_i$) and output ($\hat{\bar{K}}_o$) rays, can be written as

$$\hat{\bar{K}}_O = \frac{\lambda}{2\pi}\bar{\nabla}\phi_o \quad \text{and} \quad \hat{\bar{K}}_i = \frac{\lambda}{2\pi}\bar{\nabla}\phi_i \tag{2}$$

and the grating vector $\bar{K}_h$ as

$$\bar{K}_h = \frac{\lambda}{2\pi}\bar{\nabla}\phi_h = \frac{\lambda}{\Lambda_x}\hat{x} + \frac{\lambda}{\Lambda_y}\hat{y} \tag{3}$$

where $\bar{\nabla}$ is the gradient operator, Λ_x and Λ_y are grating spacing in the x- and y-directions, and λ is the readout wavelength. The diffraction relations can now be written as

$$\hat{K}_{x_o} = \hat{K}_{x_i} - K_{x_h} \tag{4}$$

$$\hat{K}_{y_o} = \hat{K}_{y_i} - K_{y_h} \tag{5}$$

$$\hat{K}_{z_o} = \pm\sqrt{1 - \hat{K}_{x_o}^2 - \hat{K}_{y_o}^2} \tag{6}$$

Note, $\hat{K}_{x_o}^2 + \hat{K}_{y_o}^2$ should be less than one so as not to obtain evanescent wavefronts.

The goal when designing DOEs is to transfer input rays into corresponding output rays that will be optimized for a given range of input parameters. The input parameters could, for example, either be the direction cosines of the incoming waves or the location of the input point sources. For a single specific input parameter, it is relatively easy to form a DOE that will yield the exact desired output rays. However, for a range of input parameters, it is necessary to optimize the grating vector so as to minimize the difference between the actual and the desired output rays. The optimization is achieved by minimizing the mean-squared difference between these two sets of rays [15–18].

To simplify the presentation of our optimization method, we will describe the method in one-dimensional notation. The mean-squared difference of the propagation vectors is defined as

$$E^2 = \int_{-D}^{D} \int_{a_1(x)}^{a_2(x)} \left(\hat{K}_{x_d}(x, a) - \hat{K}_{x_o}(x, a)\right)^2 da\, dx \tag{7}$$

where x is the space coordinate on the HOE, and the direction cosines of the output and desired rays, $\hat{K}_{x_o}(x, a)$ and $\hat{K}_{x_d}(x, a)$, depend on some input parameter a. The limits of integration, $a_1(x)$ and $a_2(x)$, represent the upper and lower values of the parameter of the input waves that intercept the DOE at a point x, respectively. The aperture of the DOE is $2D$. Inserting Eq. (4) into Eq. (7) yields

$$E^2 = \int_{-D}^{D} \int_{a_1(x)}^{a_2(x)} \left(\hat{K}_{x_d}(x, a) - \hat{K}_{x_i}(x, a) + K_{x_h}(x)\right)^2 da\, dx \tag{8}$$

The optimal grating vector component $K_{x_h}(x)$ can be determined by minimizing E^2 in Eq. (8). However, because the integrand is always positive, it is sufficient to minimize a simpler integral that we denote by $e^2(x_0)$, as

$$e^2(x_0) = \int_{a_1(x_0)}^{a_2(x_0)} \left(\hat{K}_{x_d}(x_0, a) - \hat{K}_{x_i}(x_0, a) + K_{x_h}(x_0)\right)^2 da \tag{9}$$

where x_0 represents an arbitrary coordinate x. Differentiating $e^2(x_0)$ with respect to $K_{x_h}(x_0)$ and setting the result to zero yield the optimal grating vector component

$$K_{x_h}(x) = \frac{-1}{(a_2(x) - a_1(x))} \int_{a_1(x)}^{a_2(x)} \left(\hat{K}_{x_d}(x, a) - \hat{K}_{x_i}(x, a)\right) da \tag{10}$$

Since the second derivative of e^2 is greater than zero, the optimal grating vector yields minimum e^2. Now, the corresponding optimal grating function can be found by using Eq. (3) to find

$$\phi_h(x) = \frac{2\pi}{\lambda} \int K_{x_h}(x)\, dx \tag{11}$$

For an on-axis holographic element that has circular symmetry, it is possible to approximate the two-dimensional grating function by one-dimensional on-axis design as

$$\phi_h(x, y) = \phi_h(r) = \frac{2\pi}{\lambda} \int K_{r_h}(r)\, dr \tag{12}$$

where $r = \sqrt{x^2 + y^2}$. For an off-axis HOE, where the off-axis angle, θ_r, is relatively low, it is possible to obtain an approximate solution by simply adding a linear term to the on-axis design to get

$$\phi_h(x, y) = (\phi_h(r))_{\text{on-axis}} + \frac{2\pi}{\lambda} \alpha_r x \tag{13}$$

where $\alpha_r = \sin \theta_r$. Finally it is possible to obtain better approximations for a general two-dimensional grating function, but at the price of added complexity [17]. Note that for a unique solution for a two-dimensional grating function, the condition of $\nabla_\perp \times \bar{K}_h = 0$ must be fulfilled, where the gradient $\nabla_\perp$ denotes $(\partial/\partial x)\hat{x} + (\partial/\partial y)\hat{y}$. This condition can be written explicitly as

$$\frac{\partial K_{x_h}(x, y)}{\partial y} = \frac{\partial K_{y_h}(x, y)}{\partial x} \tag{14}$$

A vector that fulfills this condition is known as a conserving vector. For an on-axis element that has circular symmetry, this condition is always fulfilled. However, for off-axis elements the conservation condition is not always fulfilled, so an exact solution for the grating function $\phi_h(x, y)$ cannot be found. Nevertheless, it is possible to obtain approximate solutions [17].

Optimal Diffractive Focusing Element

The operation of an on-axis diffractive focusing element is described with the aid of the one-dimensional representation in Figure 1. Here each input plane wave converges at the output plane to a point whose location corresponds to the angular direction of the input wave. The *diffractive focusing element* (DFE) has an aperture of $2D$; a focal length f, which is the distance from the element to the stop aperture and to the output plane; and is centered along the optical axis z. It also has an input stop aperture of $2W$.

It is convenient when designing a focusing element to let the input parameter, a, be the direction cosine of the input plane wave, so

$$a = \alpha = \sin \theta_i \tag{15}$$

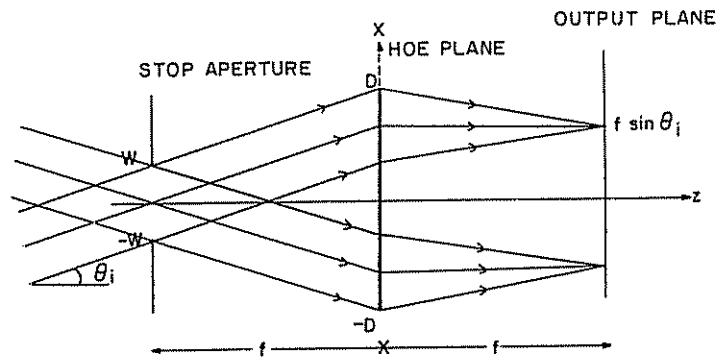

Figure 1. The readout geometry for an on-axis diffractive focusing element.

Consequently, the normalized propagation vector of the input rays is

$$\hat{K}_{x_i}(x, a) = \hat{K}_{x_i}(\alpha) = \alpha \tag{16}$$

Now, an input plane wave that has a direction cosine α must be transformed into a spherical wave converging to a point αf. Thus, the direction cosines of the desired output rays become

$$\hat{K}_{x_d}(x, a) = \hat{K}_{x_d}(x, \alpha) = \frac{-(x - \alpha f)}{\sqrt{(x - \alpha f)^2 + f^2}} \tag{17}$$

Substituting $\hat{K}_{x_i}$ from Eq. (16) and $\hat{K}_{x_d}$ from Eq. (17) into Eq. (10) yields

$$K_{x_h}(x) = \frac{-1}{(\alpha_2(x) - \alpha_1(x))} \int_{\alpha_1(x)}^{\alpha_2(x)} \left(\frac{-(x - \alpha f)}{\sqrt{(x - \alpha f)^2 + f^2}} - \alpha \right) d\alpha \tag{18}$$

where $\alpha_1(x)$ and $\alpha_2(x)$ are the lower and upper direction cosines of the input plane waves that intercept the focusing element at a point x. The analytic solution of Eq. (18) provides the final diffractive grating vector [16], from which, by using Eqs. (12) and (13), we find the grating function.

To evaluate the performance of the optimally designed focusing element, we performed a ray-tracing analysis, using Eqs. (4)–(6); the parameters of the element were chosen as $f = 100$ mm, $W = 5$ mm, $D = 15$ mm, and $\theta_r = 20°$. For comparison, we also performed a ray-tracing analysis on a conventional, nonoptimized, diffractive spherical elemental having the same parameters, for which

$$(\phi_h(x, y))_{sph} = \frac{2\pi}{\lambda} \left(\sqrt{x^2 + y^2 + f^2} + \alpha_r x \right) \tag{19}$$

The results of the analysis, which do not take into account the diffraction from the aperture, are given as spot diagrams in Figure 2 for nine discrete input angles $(\theta_{x_i}, \theta_{y_i})$. The spot diagrams for the optimized DFE are given in Figure 2*a*. The spot diagrams for the spherical element are given in Figure 2*b*. As shown, except for the central point, where the recording and readout geometries are identical for the spherical element, the results for our designed element are uniformly superior.

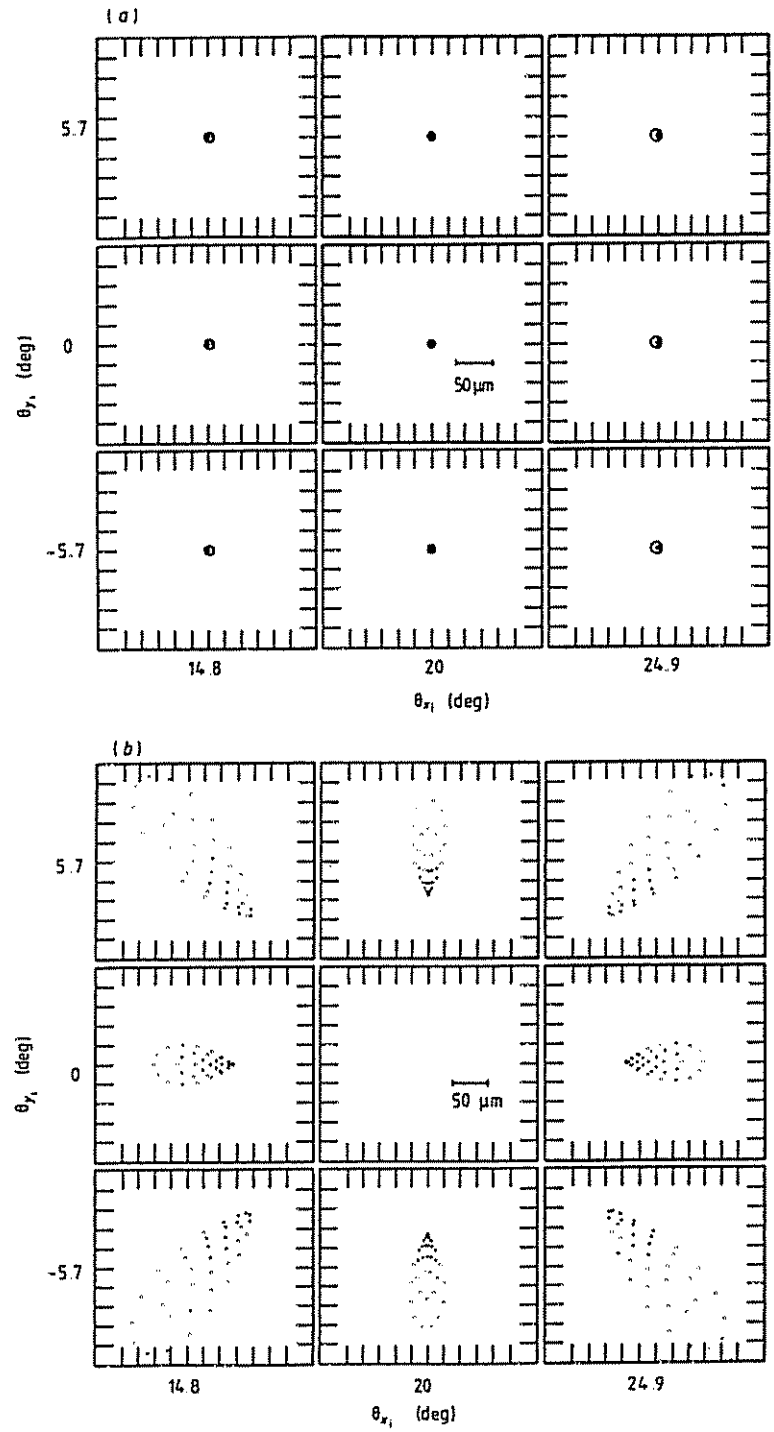

Figure 2. Spot diagrams for the off-axis DFE: (*a*) optimized grating function, (*b*) conventional spherical grating function.

Relatively small spot diagrams are obtained in the designed element, even at the extreme angles.

We also calculated the amount of distortion by subtracting the actual (average) location of each spot from the desired location; the desired focusing location of the input plane wave at θ_{x_i} is $(\alpha - \alpha_r)f$. Figure 3 shows the distortion as a function of the input angle θ_{x_i} for the one-dimensional calculation. As shown, the distortions for the optimized element are significantly smaller than those for the spherical element.

The design method was successfully illustrated by actually recording and experimentally testing aspheric reflective and transmissive focusing elements for a 10.6-μ wavelength having diffraction limited performance over a broad range of incidence angles [16, 17].

Efficient Multilevel Phase DOEs

Computer-generated DOEs can be formed so they behave as very sophisticated optical elements [7–10]. For practical optical systems the DOEs must have high diffraction efficiency. The high efficiency can be obtained by resorting to phase rather than absorptive DOEs, where the phase DOEs are recorded as etched relief patterns on a substrate. The recording can be performed by means of lithographic techniques, which are used in microelectronics. When coating the relief pattern with a reflective metallic layer, a reflective phase DOE is obtained. When the relief pattern is in a transparent material, a transmittive phase DOE is obtained.

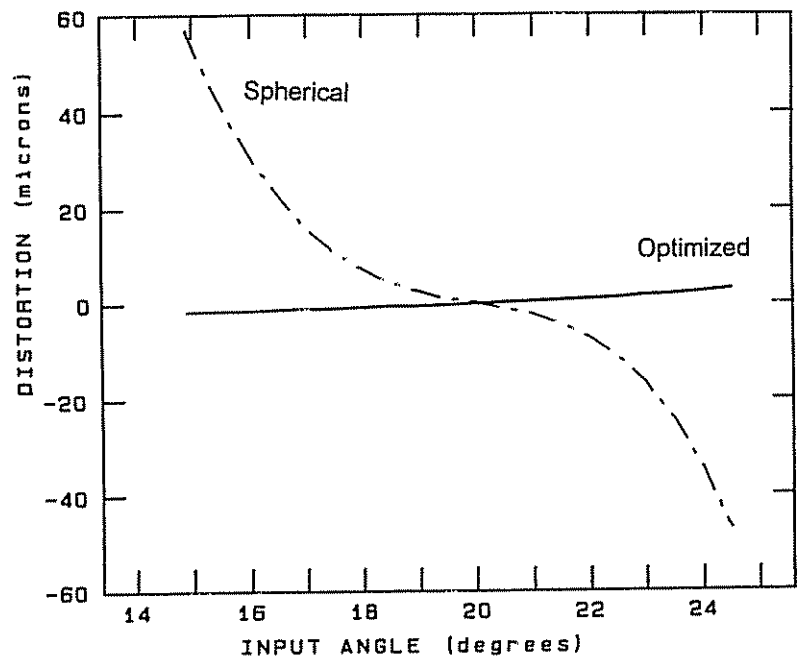

Figure 3. The distortion as a function of input angle, θ_{x_i}, for the optimized and spherical grating functions.

The diffraction efficiencies of blazed relief patterns, namely, kinoforms [11], can reach 100%. The relief height of the kinoforms are proportional to phase residues after modulo 2π, so their variations ranges from 0 to 2π. An early fabrication process for obtaining the desired surface relief involved a single photomask with variable optical density for controlling the etching rate of some substrate [11, 19]. Unfortunately, such a process does not provide the needed accuracies for controlling the graded shape and the depth of the surface relief grooves. Consequently, the single photomask with the variable density was replaced by a multiplicity of simpler binary photomasks, so the graded shape is approximated by multilevel binary steps [20, 21]. To ensure that high diffraction efficiencies are obtained, the errors due to the depth and width of the step levels must be taken into account.

In the following, we consider the basic relations that describe the performance of kinoforms and multilevel DOEs. We also record and experimentally test diffractive focusing lenses at a 10.6μ wavelength and show that high diffraction efficiencies can be reached [22–24].

Predicted Diffraction Efficiencies

The diffraction efficiency for kinoforms and multilevel elements can be calculated by using the scalar approximation. Such an approximation is valid only for a "thin" grating, for which the parameter Q [22] is much less than one; otherwise, the diffraction efficiency should be solved directly from the basic Maxwell equations [25].

In the scalar region, when a diffractive element is illuminated with a normally incident plane wave, the output wavefront will have the same form as the element, given by

$$H = \exp[iF(\phi_h)] \tag{20}$$

where ϕ_h is the desired grating function and $F(\phi_h)$ is the actual phase function of the DOE. The grating function $F(\phi_h)$ is periodic in ϕ_h, so we can expand H in a Fourier series. The Fourier expansion of Eq. (20) is given by

$$\exp[iF(\phi_h)] = \sum_{l=-\infty}^{\infty} C_l \exp[il\phi_h] \tag{21}$$

where C_l is the lth-order coefficient of the Fourier expansion, given by

$$C_l = \frac{1}{2\pi}\int_0^{2\pi} \exp[iF(\phi_h) - il\phi_h]\, d\phi_h \tag{22}$$

The diffraction efficiency, η_l, of the lth diffracted order is given by

$$\eta_l = |C_l|^2 \Big/ \sum_{k=-\infty}^{\infty} |C_k|^2 \tag{23}$$

where, for a pure phase element, $\sum_{k=-\infty}^{\infty}|C_k|^2 = 1$.

The division of the desired phase ϕ_h to N equal steps is shown in Figure 4, where the actual quantized phase $F(\phi_h)$ is given as a function of the desired phase ϕ_h. Solving Eq. (23) for the relevant first diffracted order ($l = 1$) and substituting the quantized phase $F(\phi_h)$ from Figure 4 yield the diffraction efficiency for the first diffracted order as a function of the number of levels N as

$$\eta_1 = |C_1|^2 = \left[\frac{N}{\pi}\sin\left(\frac{\pi}{N}\right)\right]^2 \tag{24}$$

Equation (24) indicates that, for 2-, 4-, 8-, and 16-phase quantization levels, the diffraction efficiency will be 40.5, 81.1, 95.0, and 98.7%, respectively.

Multilevel phase DOEs can be realized with multilevel lithography, where the surface of the DOEs needs only be etched m times in order to obtain $N = 2^m$ levels. A different mask is used for each etch step, with a desired depth for each etch being

$$\Delta_m = \frac{\lambda}{\Delta n\, 2^m} \tag{25}$$

where λ is the wavelength and Δn is the relief modulating refractive index change for transmissive elements and $\Delta n = 2$ for reflective elements. The amplitude transmittance for the mth mask is given by

$$t_m = U_s\left[\sin(2^{m-1}\phi_h)\right] \tag{26}$$

where

$$U_s(\xi) = \begin{cases} 1 & \text{when } \xi \geq 0 \\ 0 & \text{when } \xi < 0 \end{cases}$$

We now consider, by using Eq. (22), how the depth errors due to improper level etching, and the width errors due to misalignment of the masks, affect the diffraction efficiency [22]. Figure 5 shows the efficiency as a function of the relative etch depth error δ_d for $N = 2, 4, 8, 16$, and infinity levels. As shown, there is only a slight reduction of diffraction efficiency when the depth error is less than 10%.

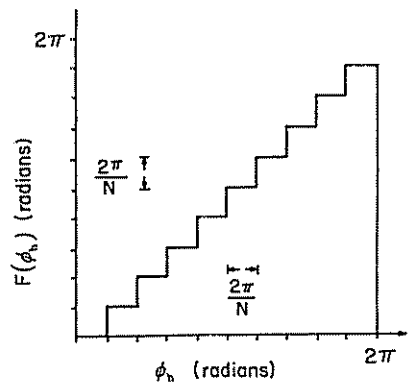

Figure 4. Actual quantized phase $F(\phi_h)$ as a function of the desired phase ϕ_h.

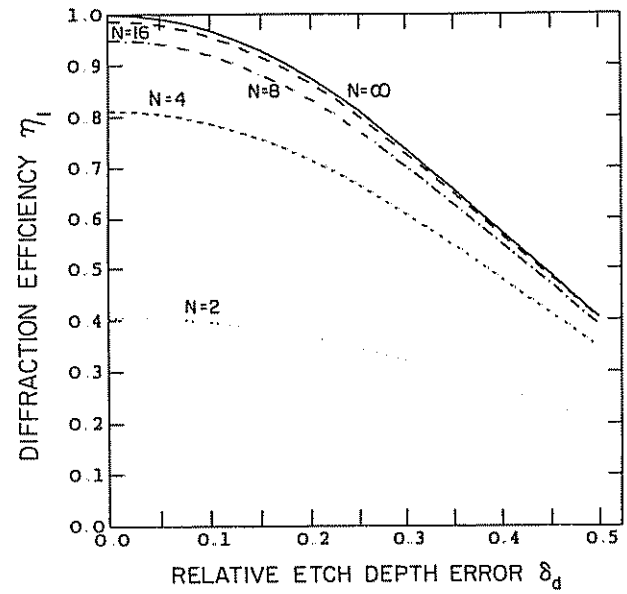

Figure 5. Diffraction efficiency η_t as a function of the relative etch depth error δ_d for $N = 2, 4, 8, 16$, and infinity step levels.

However, as the error increases beyond 10%, the reduction in efficiency becomes significant. The reduction of the diffraction efficiency as a function of horizontal misalignment relative to the minimal width of the step levels, δ_w is shown in Figure 6 for $N = 2, 4, 8, 16$ levels. Again, relative misalignment of less than 10% does not cause any significant reduction in the diffraction efficiencies.

Realization Procedure and Experimental Results

We recorded a multilevel diffractive focusing element for a 10.6-μ wavelength with 15-mm diameter and 150-mm focal length [22]. The desired relief pattern was obtained by multilevel lithography with the use of several masks. Each mask was first plotted as a binary computer-generated hologram in accordance with Eq. (26) using a laser scanner (Scitex Raystar, Response 300) that had a resolution capability of approximately 10μ and was then recorded onto a photographic film. The plots were demagnified optically and recorded as chrome master masks. The information from each mask was then transferred by contact printing and suitable exposure onto a single crystal GaAs wafer, coated with an approximately 1-μ photoresist layer. After the photoresist was developed, the GaAs was etched and the remaining photoresist was removed. The etch depth of the mth mask was determined according to Eq. (25).

We recorded a reflective focusing lens with 8 levels and a transmissive focusing lens with 16 levels. For the reflective element, the etched GaAs wafer was overcoated with a thin gold layer, where for the transmissive element both the etched surface and the back planar surface were overcoated with antireflection layers. Representative surface profilometer traces for etched sections of these diffractive focusing lenses are presented in Figure 7. Figure 7*a* depicts the 8 levels

of the reflective element, and Figure 7*b* depicts the 16 levels of the transmissive element.

We experimentally evaluated the two focusing lenses by measuring their diffraction efficiencies and focused spot sizes. The measured diffraction efficiency for the reflective element was 88 ± 1% rather than the theoretical value of 95%, whereas for the transmissive element the measured diffraction efficiency was 87 ± 1% rather than the 98.7% of the theoretical value. We attribute the loss in efficiency to improper depths and misalignment errors as well as to insufficient loss reduction by the antireflection coating in the transmissive lens. The focused spot sizes for both the transmissive and reflective lenses were measured using the scanning knife edge method. The results indicated that the spot size is 260μ, which is the expected diffraction limited size for these lenses.

Hetrostructure Multilevel Binary Optics

The fabrication processes for DOEs rely mainly on etching techniques that are difficult to control accurately. As a result, the shape and depth of the grooves can differ from those desired, which leads in reductions of diffraction efficiency and poor repeatability of performance, as indicated by Figure 5. We developed a method for forming multilevel diffractive elements that have highly accurate level heights so as to obtain high diffraction efficiencies. The method, which we named *Hetrostructure Multilevel Binary Optics* (HMBO), relies on conventional deposition technology, selective etching, and multimask lithography [23]. With deposition, rather than etching, it is possible to achieve extremely accurate control of the level depths.

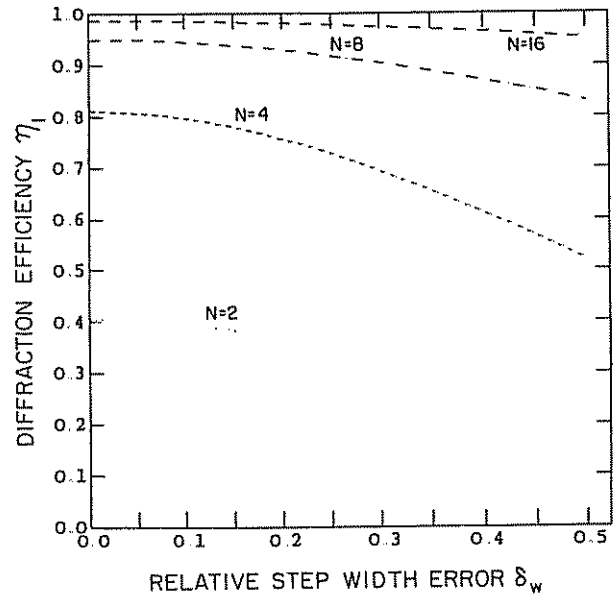

Figure 6. Diffraction efficiency η_1 as a function of the relative step width error δ_w for N = 2, 4, 8, and 16 step levels.

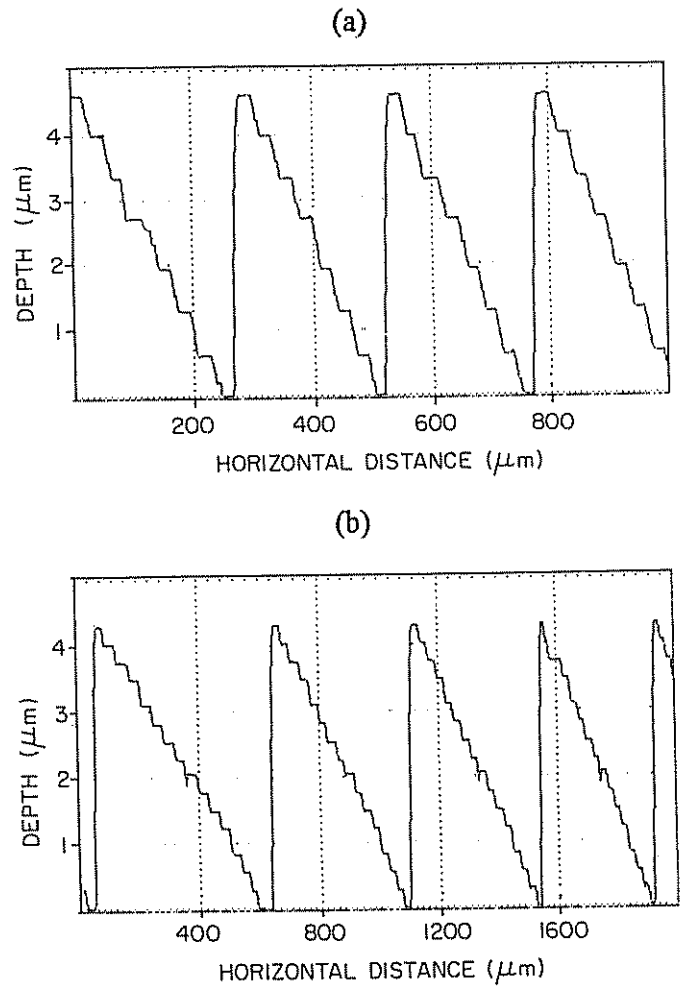

Figure 7. Surface profilometer traces for typical etched solutions of a diffractive focusing lens: (*a*) 8 levels of the reflective element and (*b*) 16 levels of the transmissive element.

Our process for forming HMBO is described with the aid of Figure 8. Two materials, denoted A and B, are deposited alternately to form the multilevel hetrostructure. Each pair of layers (A + B) forms a single level, of thickness Δ, which is determined according to

$$\Delta = \frac{\lambda}{N\Delta n} \tag{27}$$

By exploiting multimask lithography and selective etching techniques, in which one of the layers' material acts as a stop, it is possible to obtain a multiplicity of levels, each having a depth that can be controlled with high accuracy.

To illustrate the effectiveness of our process, we recorded a reflective HMBO focusing lens for 10.6-μ radiation. Only four levels ($N = 4$) were formed, so only two masks were needed. Aluminum and Ni-Cr (80:20) were chosen as the alterna-

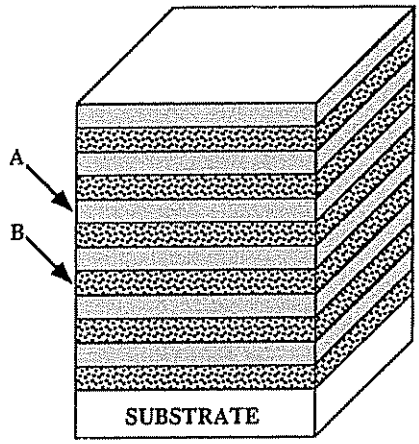

Figure 8. Multilevel hetrostructure configuration.

tive materials denoted B and A in Figure 8. We found etchants for which the Ni-Cr acts as a stop layer for the aluminum etchant, while the aluminum serves as a stop layer for the Ni-Cr etchant [23].

The formation procedure of the HMBO lens is illustrated in Figure 9. The first UV exposure is shown in Figure 9*a*; the first etching step, in Figure 9*b*; the second UV exposure, in Figure 9*c*; and, finally, the second etching step, in Figure 9*d*.

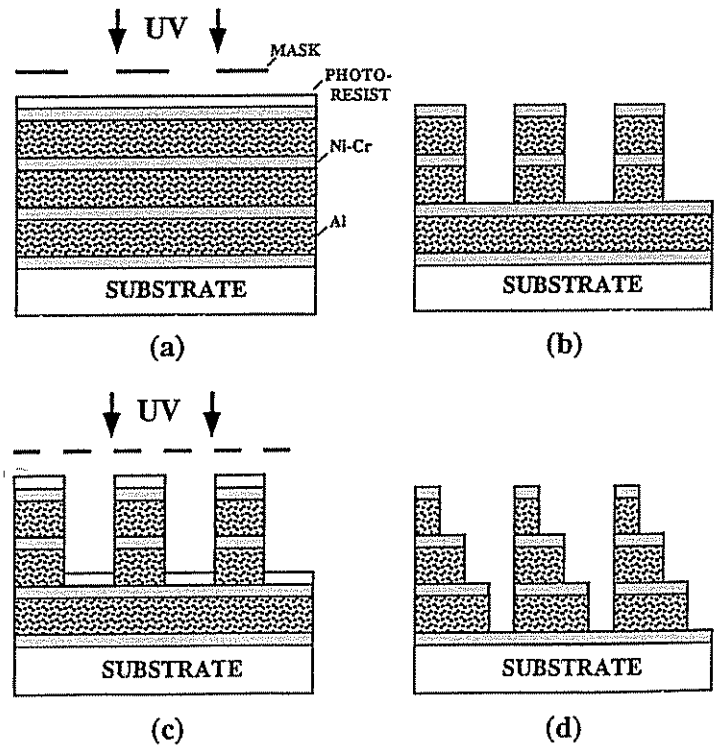

Figure 9. The HMBO fabrication process: (*a*) the first UV exposure, (*b*) the first etching step, (*c*) the second UV exposure, (*d*) the second etching step.

Several HMBO lenses were recorded, and their diffraction efficiencies and resolution capabilities were measured. We found that the performance of all lenses was highly repeatable, where the diffraction efficiency was close to the theoretical value of 81.1% as given by Eq. (24) for four levels, and the resolution capability is also the predicted diffraction limit value. By increasing the number of levels, it would of course be possible to reach diffraction efficiencies close to 100%.

Generalized Multilevel DOEs

The diffraction efficiency of multilevel DOEs depends on the shape and the height of every level, where for best efficiency, the level height must be varied according to the period of the grating and the angle of the incident beam [24]. For a DOE that has a variety of periods, such as a high numerical aperture diffractive lens, it is not possible to arbitrarily change the height of a level for each specific period. Consequently, the overall diffraction efficiency for such DOEs is relatively low. Moreover, by utilizing conventional design methods, it is difficult to vary independently the phase and the amplitude of the output wavefront, as is sometimes necessary for some applications such as matched filtering and subdiffraction limited focusing lenses.

We developed a new approach to design computer-generated multilevel diffractive elements in which the phase and the amplitude of the output wavefront can be controlled independently [26]. The approach is based on varying the local diffraction efficiency by changing the width and the number of levels in every period. Indeed, the diffraction efficiency of the elements can be arbitrarily controlled to reach 100% over the entire element.

To illustrate how to vary independently the amplitude and phase of the wavefront that emerges from a DOE, we designed and recorded a specific cylindrical DOE for which the intensity along the line at the focus should increase linearly. For the recording of DOE, we exploited conventional lithographic techniques with wet chemical etching for transferring the mask data onto a GaAs substrate. The size of the final DOE was 30 mm by 30 mm and its focal length was 240 mm. The arrangement of the DOE together with the incident plane wave and converging output wavefront is schematically shown in Figure 10. The intensity distribution at the focus was measured at a 10.6-μ wavelength using a slit that was translated by a stepper motor and the light, which passing through the slit at each location was

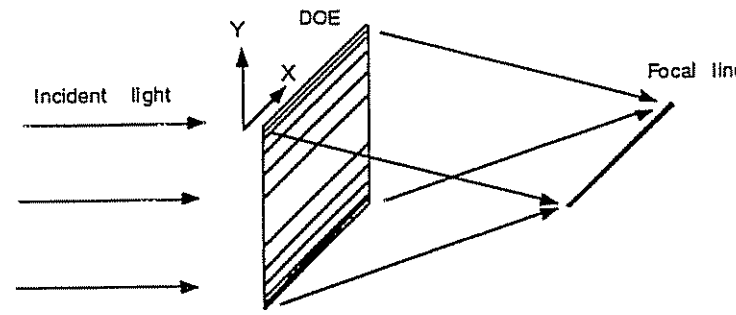

Figure 10. Geometry of the incident and output wavefronts from a cylindrical DOE.

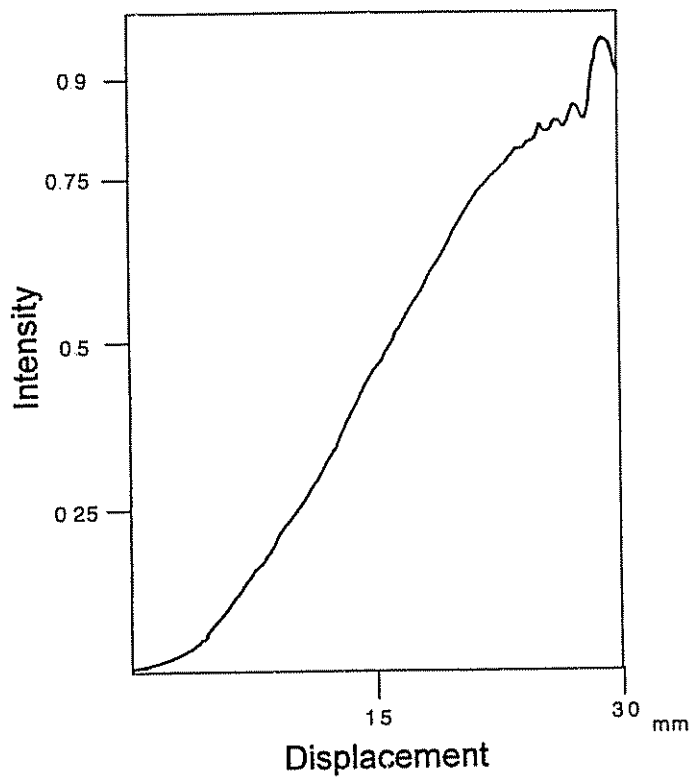

Figure 11. Measured intensity distribution along the line at the focus plane.

collected onto a thermal detector. Figure 11 shows the quantitative measurements with the scanned slit and thermal detector. As evident, the intensity distribution along the focus is indeed linear as expected, indicating that independent control of the amplitude and phase of the output wavefront was indeed achieved. Deviation from linearity at the high-intensity levels is attributed to diffraction at the edges of the DOE.

Blazed Gratings for Polychromatic and Multidirectional Incidence Light

An important consideration for surface relief gratings is that their diffraction efficiencies must be as high as possible. When the gratings are illuminated with a beam at a specific wavelength and a specific angle of incidence, it is possible to obtain 100% diffraction efficiency with properly blazed groove shapes. However, when the beam is polychromatic or incident at orientation angles different from those for which the blazing was designed, the diffraction efficiency is reduced substantially. Nevertheless, it is possible to optimize the groove depth of blazed gratings [24]. The approach is based on calculating the diffraction efficiency as a function of the incidence angle, the wavelength, and the groove depth and then choosing the depth that maximizes the overall diffraction efficiency over the entire range of angles and wavelengths.

It is possible to obtain a diffraction efficiency of 100% with a maximal groove depth of

$$d_{\text{opt}} = \frac{\lambda}{n_1\cos(\theta_i) - n_2\cos(\theta_o)} \tag{28}$$

where θ_i and θ_o are the angular orientations of the incident wave and that of the diffracted wave respectively, n_1 is the refractive index of the surrounding medium, and n_2 is the refractive index of the grating medium for a reflective grating $n_1 = -n_2$. However, at other angles and wavelengths, the diffraction efficiency is reduced considerably.

As an illustration, we calculated the diffraction efficiency for incidence angles ranging from $-45°$ to $45°$. The grating period was $\Lambda = 30\lambda$, and the groove depth was $d = \lambda/2$ (appropriate for normal incidence). The results are shown in Figure 12, together with the results obtained from a rigorous vectorial formalism in which TE polarization was assumed [25]. As shown, good agreement exists between the scalar and the vectorial results, and both predict a decrease of as much as 25% in the diffraction efficiency at the extreme angles. In accordance with our procedure [24], the optimal groove depth for the range $-45° < \theta < 45°$ is $d_{\text{opt}} = 0.55\lambda$. Figure 13 shows the diffraction efficiency as a function of the angle of incidence for a grating having the optimal groove depth. Comparing Figures 12 and 13, it is evident that, for the grating with the optimal groove depth, the diffraction efficiencies are more uniform over the range of angle.

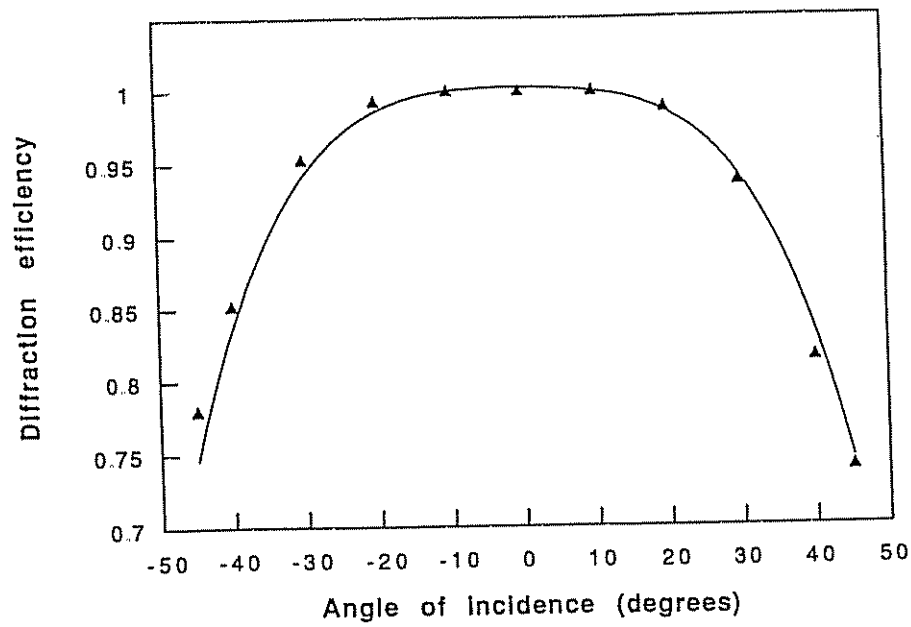

Figure 12. Calculated diffraction efficiency as a function of the angle of incidence for a blazed grating with a groove depth of 0.50λ. Curve: scalar calculation; triangles: vectorial calculation.

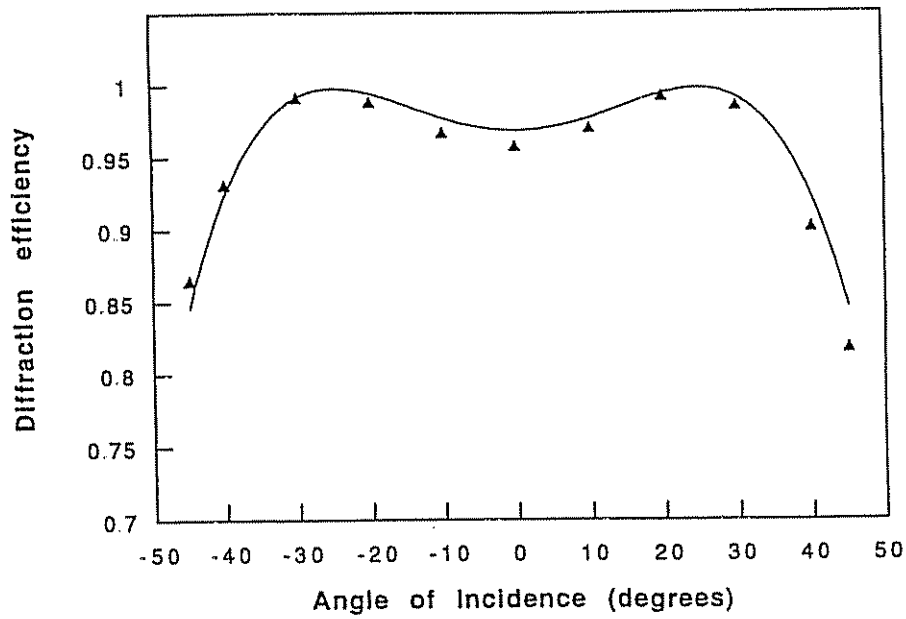

Figure 13. Calculated diffraction efficiency as a function of the angle of incidence for a blazed grating with a groove depth of 0.55λ (optimal depth). Curve: scalar calculation; triangles: vectorial calculation.

Possible Applications for DOEs

In the following, we briefly review a number of applications in which DOEs have been successfully incorporated.

Optical Coordinate Transformation

Diffractive optical elements can perform coordinate transformations [27] that can be exploited for distortion compensation, for angle multiplexing in optical fibers, and for optical data processing.

An optical arrangement for realizing a general two-dimensional coordinate transformation $(x, y) \rightarrow [u(x, y), v(x, y)]$ is shown schematically in Figure 14. A DOE that has a grating function of $\phi_h(x, y)$ is placed adjacent to an amplitude transmission function of $f(x, y)$. The desired coordinate transformation $F(u, v)$ is obtained at some distance z away. To find the necessary grating function for the DOE, it is most convenient to find its grating vector first using the propagation vectors of the input and output wavefronts [28–30]. This grating vector has the form

$$K_{x_h}(x, y) = \frac{u(x, y) - x}{r} \tag{29}$$

$$K_{y_h}(x, y) = \frac{v(x, y) - y}{r} \tag{30}$$

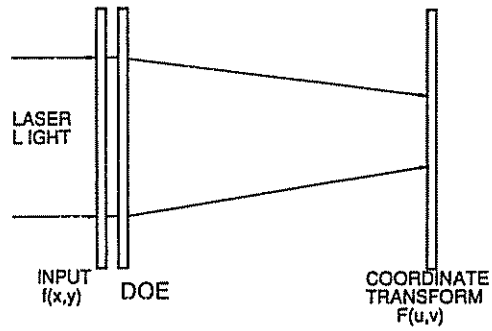

Figure 14. Coordinate transformation arrangement with a DOE.

where

$$r^2 = [u(x, y) - x]^2 + [v(x, y) - y]^2 + z^2 \tag{31}$$

Then, the grating function is determined using Eqs. (12) and (13).

As an illustration, we consider how DOEs can be exploited for transforming an annular laser beam to a uniform circular beam [31]. The optical arrangement, consisting of two DOEs, is schematically shown in Figure 15. The first DOE converts an incident annular beam with uniform intensity and phase into a circular beam with uniform intensity at the position of the second DOE. The second DOE then serves as phase corrector to produce a uniform output phase.

For the experiment, only the first DOE was recorded as a transmission surface relief grating with 16 discrete binary levels. The recording involved four binary masks and multiple lithographic processes. The DOE was tested with a 10.6-μ wavelength derived from a CO_2 laser. The results are presented in Figure 16. Figure 16*a* shows the light intensity distribution at the input, and Figure 16*b* shows

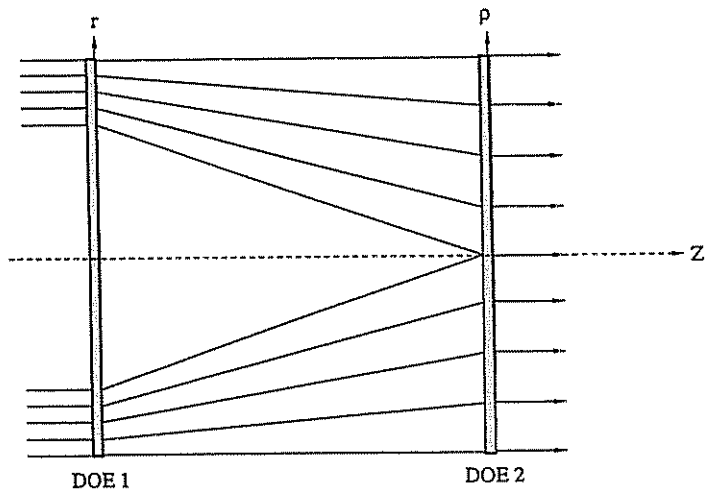

Figure 15. Optical arrangement consisting of two diffractive optical elements for transforming an annular laser beam into a uniform one.

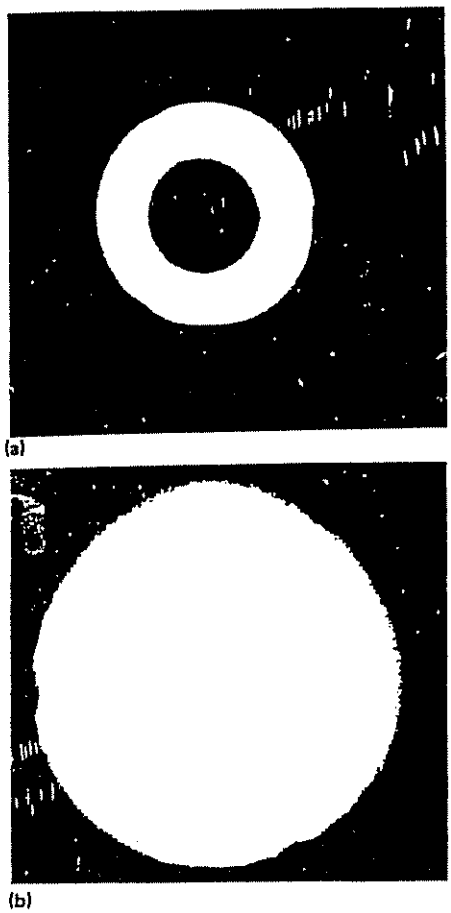

Figure 16. Experimental light intensity distribution for annular to uniform beam transformation: (*a*) input and (*b*) output.

the light intensity distribution at the output. As can be seen, the shapes of the intensity distributions are indeed as expected.

These investigations also led to the development of a technique for forming nondiffracting beams having essentially constant intensity along the propagation direction [32]. Two phase-only DOEs were exploited to form the nondiffractive beam as well as to obtain a high diffraction efficiency.

Hybrid Diffractive-Refractive Achromats

Diffractive and refractive elements can be combined to eliminate, or at least significantly reduce, chromatic aberrations. These so-called hybrid achromats exploit the fact that the dispersion of refractive elements is opposite that of diffractive elements, so they can cancel each other. The attractive aspect of hybrid achromats is that, unlike wholly refractive achromats, they require only one type of refracting material, and the curvatures of the refractive surfaces are not as extreme.

We investigated analytic design procedure [33] for hybrid achromats that combine refractive and diffractive elements of the form shown in Figure 17. The design procedure involves two separate stages. In the first stage the chromatic aberrations are corrected for the paraxial rays, and in the second stage the spherical aberrations are corrected by the addition of an aspherical phase function with the diffractive element. We illustrated the design procedure by designing a plano-convex achromat having little chromatic dispersion at 10.6-μ radiation.

Multiple Beam Grating

Diffractive optics can also be exploited for producing novel binary phase relief gratings, having characteristics that cannot be matched with conventional optics. One example is a multiple beam grating, whose function is to produce an array of equal intensity beams from a single input beam. The grating function in this case corresponds to the interferenced pattern formed by an array of point sources at infinity. By controlling the fringe location, spacing, and duty cycle of a binary phase grating, a specified array of beams can be produced when illuminating the grating with a single beam.

The multiple beam grating design method was exploited for designing specific gratings that are useful for a 10.6-μ wavelength [34]. Such gratings were recorded with the aid of computer-controlled laser scanners and photolithographic techniques. Reflective and transmissive elements were formed by either etching reflective metal layers or GaAs substrates. The actual far-field intensity distribution for a representative reflective grating that can produce 20 output beams, with beam separation of 2 mrad, is shown in Figure 18. As measured, the root mean square variation of the beam intensities was 5.5%.

Diffractive Axilens: High Resolution and Long Focal Depth

Optical elements that have both long focal depth as well as high lateral resolution are needed for a variety of applications, including precision alignment and profile measurements [35]. Conventional elements (such as spherical lenses and mirror) cannot achieve these two goals simultaneously; high lateral resolution requires

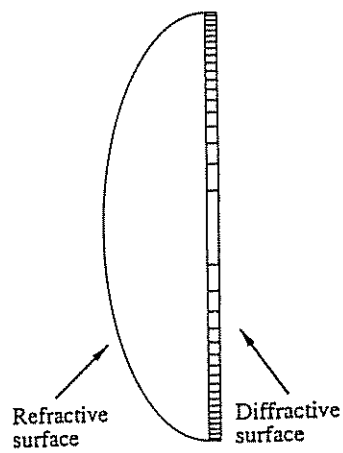

Figure 17. Schematic representation of a hybrid diffractive-refractive achromat.

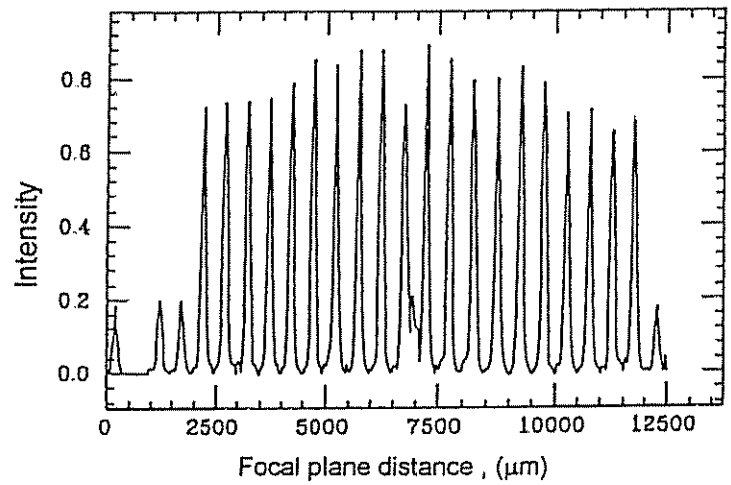

Figure 18. Far-field intensity distribution for a multiple beam grating.

high numerical apertures, whereas long depth of focus requires low numerical apertures.

We investigated special aspheric DOEs that can have arbitrarily long focal depth as well as high lateral resolution [36]. This element essentially combines the properties of the long focal depth of an axicon and the high energy concentration of a conventional spherical lens, so we named it axilens. The grating of such an axilens has the form

$$\phi_h(r) = \frac{2\pi}{\lambda}\frac{r^2}{2f(r)} \tag{32}$$

where r is the radial coordinate of the element, λ is the wavelength of the light, and $f(r)$ is a continuous function instead of constant for a simple lens. The variable focal length $f(r)$ may be the monotonic function

$$f(r) = f_0 + ar^b \tag{33}$$

where, a, b, and f_0 are constants. The constant a in Eq. (33) can be expressed in terms of the desired focal depth of the element as

$$a = \frac{\delta z_g}{R^2} \tag{34}$$

where R is the radius of the DOE and δz_g is the focal depth. The constant b depends on the desired intensity distribution of the central peak. For example, $b = 2$ in the case of uniform intensity distribution of the central peak throughout the focal range. The geometrical parameters and the distribution of rays for such an axilens are shown in Figure 19. For the experiment, we derive the phase function for a specific axilens, record it as a computer-generated hologram, and then verify the numerical simulations experimentally [36].

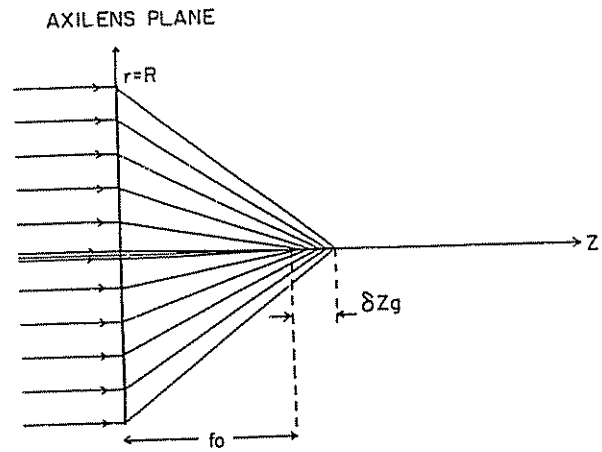

Figure 19. Geometrical parameters and schematic distribution of rays with an input plane wave focused by an axilens.

Computer-Generated Relief Gratings as Space-Variant Polarization Elements

Transmissive relief linear gratings of ultrahigh spatial frequencies can behave as homogeneous birefringent materials. Sometimes, however, elements that can perform nonuniform, space-variant polarization are required, for example, elements for transforming the azimuthal polarization of high-power annular CO_2 laser beams into linearly polarized beams, and elements for polarization coding of the data in optical computing [37].

We investigated a method for exploiting nonuniform relief grating for space-variant polarization elements [38]. In this method the local direction of the gratings determines the polarization angles, while the period of the gratings is controlled to ensure continuity of the grating function for any desired polarization operation. Our method was then illustrated with a specific space-variant half wave plate that transforms a wavefront (CO_2 laser) with uniform linear polarization into one with nonuniform polarization.

Concluding Remarks

We have shown that it is possible to optimize the design and recording of diffractive optical elements so they can be operated at a variety of wavelengths over a broad range of incidence angles and have high diffraction efficiencies. Such elements can be incorporated into a number of applications, such as coordinate transformations, beam shaping, and polarization control.

Our design and recording methods need not be confined to the examples cited in this paper but could be applicable for designing and forming a wide variety of diffractive elements. Specifically, it is possible to exploit our methods for diffractive elements that can be incorporated in general beam profile transformations, in optical scanners, in compact disks, and in imaging applications. Furthermore, the methods could be extended to deal with multielement optical systems. When including polychromatic light sources, it is possible to compensate for chromatic aberrations by combining diffractive and refractive optical elements.

Finally, we would like to note that as the design and recording technologies improve, more complex diffractive optical elements will be formed. These could have unique properties that would not be obtainable via conventional optical elements.

References

1. Leith, E. N., and J. Upatnieks. 1962. Reconstructed wavefronts and communication theory. *J. Opt. Soc. Amer.* 52:1123.
2. Leith, E. N., and J. Upatnieks. 1963. Wavefront reconstruction with continuous tone objects. *J. Opt. Soc. Amer.* 53:1377.
3. Leith, E. N., and J. Upatnieks. 1964. Wavefront reconstruction with diffused illumination and three-dimensional objects. *J. Opt. Soc. Amer.* 54:1295.
4. Gabor, D. 1948. A new microscope principle. *Nature* 161:777.
5. Gabor, D. 1949. Microscopy by reconstructed wavefronts. *Proc. Roy. Soc. A* 197:454.
6. Close, D. H. 1975. Holographic optical elements. *Opt. Engrg.* 14:408.
7. Brown, B. R., and A. W. Lohmann. 1966. Complex spatial filtering with binary masks. *Appl. Optics* 55:967.
8. Burch, J. J., 1967. A computer algorithm for the synthesis of spatial frequency filters. *Proc. IEEE* 55:599.
9. Lee, W. H. 1974. Binary synthetic holograms. *Appl. Optics* 13:1677.
10. Lee, W. H. 1978. Computer generated holograms: techniques and applications. *Prog. in Optics* 16:119.
11. Jordan, J. A., P. M. Hirsch, L. B. Lesem, and D. L. Van Rooy. 1970. Kinoform lenses. *Appl. Optics* 9:1883.
12. Fairchild, R. C., and R. J. Fienup. 1982. Computer-originated hologram lenses. *Opt. Engrg.* 21:133.
13. Winick, K. A., and J. R. Fienup. 1983. Optimum holographic elements recorded with nonspherical wavefronts. *J. Opt. Soc. Amer.* 73:208.
14. Kedmi, J., and A. A. Friesem. 1986. Optimized holographic optical elements. *J. Opt. Soc. Amer. A* 3:2011.
15. Hasman, E., and A. A. Friesem. 1989. Analytic optimization for holographic optical elements. *J. Opt. Soc. Amer. A* 6:62.
16. Hasman, E., N. Davidson, A. A. Friesem, M. Nagler, and R. Cohen. 1990. Holographic focussing elements for IR radiation. *Meas. Sci. Tech.* 1:59.
17. Hasman, E., N. Davidson, and A. A. Friesem. 1992. Aspheric holographic elements for IR radiation. *Optics Comm.* 89:306.
18. Hasman, E., and A. A. Friesem. 1991. Method of optimizing holographic optical elements. U.S.A. patent number 5,075,800, December 24, 1991.
19. Andersson, H., Mats Ekberg, Sverker Hard, Stellan Jacobsson, Michael Larsson, and T. Nilsson. 1990. Single photomask multilevel kinoforms in quartz and photoresist: manufacture and evaluation. *Appl. Optics* 29:4259.
20. d'Auria, L., J. P. Huignard, A. M. Roy, and E. Spitz. 1972. Photolithographic fabrication of thin film lenses. *Optics Comm.* 5:232.
21. Swanson, G. J., and W. B. Veldkamp. 1989. Diffractive optical elements for use in infrared systems. *Opt. Engrg.* 28:605.
22. Hasman, E., N. Davidson, and A. A. Friesem. 1991. Efficient multilevel phase holograms for CO_2 lasers. *Optics Lett.* 16:423.
23. Hasman, E., N. Davidson, and A. A. Friesem. 1991. Heterostructure multilevel binary optics. *Optics Lett.* 16:1460.
24. Davidson, N., R. Duer, A. A. Friesem, and E. Hasman. 1992. Blazed holographic grating for polychromatic and multidirectional incidence light. *J. Opt. Soc. Amer. A* 9:1196.

25. Moharam, M. G., and T. K. Gaylord. 1982. Diffraction analysis of dielectric surface relief grating. *J. Opt. Soc. Amer.* 72:1383.
26. Danziger, Y., E. Hasman, A. A. Friesem, and A. W. Lohmann. 1996. Multilevel diffractive elements for generalized wavefront shaping. *Opt. Engrg.* 35(9):2556.
27. Bryngdahl, O. 1974. Geometrical transformation in optics. *J. Opt. Soc. Amer.* 64:1092.
28. Davidson, N., A. A. Friesem, and E. Hasman. 1992. Optical coordinate transformations. *Appl. Optics* 31:1067.
29. Davidson, N., A. A. Friesem, and E. Hasman. 1992. On the limits of optical interconnects. *Appl. Optics* 31:5426.
30. Davidson, N., A. A. Friesem, E. Hasman, and I. Shariv. Curved holographic elements for optical coordinate transformations. *Optics Lett.* 16:1430.
31. Davidson, N., A. A. Friesem, and E. Hasman. Diffractive elements for annular laser beam transformation. *Appl. Phys. Lett.* 61:381.
32. Davidson, N., A. A. Friesem, and E. Hasman. 1992. Efficient formation of nondiffracting beams with uniform intensity along the propagation direction. *Optics Comm.* 88:326.
33. Davidson, N., A. A. Friesem, and E. Hasman. 1993. Analytic design of hybrid diffractive-refractive achromats. *Appl. Optics* 32:4770.
34. Friesem, A. A., N. Davidson, E. Hasman, and O. Kinrot. 1990. Advances in holographic optical elements. *SPIE* 1319.
35. Hasman, E., N. Davidson, and A. A. Friesem. 1992. Multifunctional holographic elements for surface measurements. *Opt. Engrg.* 31:363.
36. Davidson, N., A. A. Friesem, and E. Hasman. 1991. Holographic axilens: high resolution and long focal depth. *Optics Lett.* 16:523.
37. Davidson, N., A. A. Friesem, and E. Hasman. 1992. Realization of perfect shuffle and inverse perfect shuffle transforms with holographic elements. *Appl. Opt.* 31:1810.
38. Davidson, N., A. A. Friesem, and E. Hasman. 1992. Computer-generated relief grating a space-variant polarization elements. *Optics Lett.* 17:1541.

Biographies

Erez Hasman received the B.Sc. degree in 1981 from the Tel Aviv University, the M.Sc. degree in 1985 from the Technion, Haifa, and the Ph.D. in 1992 from Weizmann Institute of Science, Rehovot, Israel. From 1981 to 1986 he was employed by the government of Israel, Department of Science, Haifa. From 1992 to 1994 he was chief physicist of graphic and recognition product lines with the Optrotech Company, performing research and development in the areas of photoplotter and imaging systems for printed circuit boards and graphic arts industries. From 1994 to 1996, he was a technology analysis manager at El-Op Company in Israel and a scientific consultant at Weizmann Institute of Science. Presently, he is a senior visitor scientist at Weizmann Institute of Science and a scientific consultant. His research interests include holography, diffractive optics, optical computing, optical measurement, optical memory, and nonconventional laser resonators.

Nir Davidson received the B.Sc. Degree in 1982 from the Hebrew University, Jerusalem, and the M.Sc. degree in 1987 from the Technion, Haifa. He received a Ph.D. degree in 1992 from the Weizmann Institute of Science, Rehovot, Israel, in the field of diffractive optics. From 1992 to 1994 he was at Stanford University, conducting investigations in atomic physics and lasers. In 1994 he joined the faculty of the Weizmann Institute of Science, becoming a senior researcher in 1995. His research interests include atomic physics, laser cooling and trapping of atoms, precision measurements, and diffractive optics. He is a member of Optical Society of America, American Physics Society, and Israeli Physics Society.

Yochay Danziger received the B.Sc. degree in 1991 from the Ben Gurion University, Beer-Sheva, and the M.Sc. degree in 1995 from the Weizmann Institute of Science, Rehovot,

Israel, where he is currently pursuing his doctoral research. His research interests include diffractive optical elements, optical resonators, and far infrared applications.

A. A. Friesem received the B.Sc. and Ph.D. degrees from the University of Michigan in 1958 and 1968, respectively. From 1958 to 1963 he was employed by Bell Aero Systems Company and Bendix Research Laboratories. From 1963 to 1969 he was at the University of Michigan Institute of Science and Technology, conducting investigations in coherent optics, mainly in the areas of optical data processing and holography. From 1969 to 1973 he was principal research engineer in the Electro-Optics Center of Harris, Inc., performing research in the areas of optical memories and displays. In 1973 he joined the staff of the Weizmann Institute of Science, becoming professor of optical sciences in 1977. He is concerned with new holographic concepts and applications, optical image processing, and electro-optics devices. Friesem is a fellow of OSA, fellow IEEE, member of SPIE, past chairman of the Israel Laser and Electro-Optics Society, and a member of Eta Kappa Nu and Sigma Xi.